Microchimica Acta (2018) 185: 41
https://doi.org/10.1007/s00604-017-2561-0

ORIGINAL PAPER

Fluorometric competitive immunoassay for chlorpyrifos using rhodamine-modified gold nanoparticles as a label

Xiaowen Dou[1] · Lei Zhang[1] · Congmin Liu[1] · Qian Li[1] · Jiaoyang Luo[1] · Meihua Yang[1]

Received: 13 August 2017 / Accepted: 9 November 2017 / Published online: 8 December 2017

Abstract

A new kind of labelled antibody was synthesized by modifying gold nanoparticles (AuNPs) with the fluorophore rhodamine B isothiocyanate (RBITC) and a secondary antibody (IgG). The conjugate thus obtained was used in a competitive sandwich assay with a turn-on signal change. It was designed to detect the organophosphorus pesticide chlorpyrifos. The fluorescence of the RBITC-labeled gold immunoprobe with emission at 575 nm and excitation at 556 nm is almost completely quenched. If, however, cysteamine is added, the fluorophore is released from the labeled secondary antibody and fluorescence increases in accordance with the quantity of secondary antibody bound to the sandwich. This assay was applied to determine chlorpyrifos in dried tangerine peels. The detection results were also independently confirmed by LC-MS/MS. The method allows the concentrations of chlorpyrifos to be quantified down to 4.9 $ng \cdot mL^{-1}$, which is equivalent to 61 $\mu g \cdot kg^{-1}$ in dried tangerine peels. In our perception, this approach has a wide potential to be applied in the determination of numerous analytes for which antibodies are available.

Keywords Labeled probe · Nanoprobe · Surface-assembly · Nanogold · Rhodamine B isothiocyanate · Fluorescence immunoassay · Turn-on scheme · Organophosphorus pesticide · Labeled monitoring platform · Cysteamine

Introduction

Intensive agricultural activities have culminated in the use of toxic pesticides, which present a known, hazardous risk to human health. This is largely due to the inability to control the spread of pesticides, as they have been found in foodstuffs [1], environment [2], and even in medicinal herbs [3]. Therefore, portable detection techniques for early monitoring of trace pesticides in foodstuffs are urgently required.

Great efforts have led to the development of a variety of user-friendly biosensing systems for hazardous pesticides based on optical [4] or electrochemical [5] techniques. Electronical sensing mostly installed with complex platforms such as graphene composite film [6] and multi-horseradish peroxidase-flake like Fe_3O_4 coated carbon nanotube nanocomposites [7]. It certainly enables a high sensitivity for pesticide monitoring, but these systems require additional substrates (e.g. HRP, chitosan, protein A, dopamine) to induce the response. The optical biosensor equipped with multi-channel biochips provides a high-throughput and ultra-sensitive platform, but the chips were prepared at 1100 °C and expensive spectrum instruments were needed to fulfill these detections. This may restrict their wide use. As a promising tool both for laboratory and field analyses, fluorescence immunoassays have attracted increasing attentions in contaminant screening such as pesticides [8–10]. To achieve a sensitive detection required for small targets, this technique emphasizes the competitive antibody binding between antigen and target, thereby enables competitive readouts with tags like fluorescent dyes [10, 11], dye-modified with nanomaterials [12] and pure nanobeads [9, 13]. The reported assays generally focused on continuous fluorescence lighting, particularly in dye labeling. It tended to result in a low signal-to-

This manuscript has been thoroughly edited by a native English speaker from an editing company.

Electronic supplementary material The online version of this article (https://doi.org/10.1007/s00604-017-2561-0) contains supplementary material, which is available to authorized users.

✉ Meihua Yang
yangmeihua15@hotmail.com

[1] Key Laboratory of Bioactive Substances and Resources Utilization of Chinese Herbal Medicine, Ministry of Education, Institute of Medicinal Plant Development, Chinese Academy of Medical Sciences and Peking Union Medical College, Haidian District, Beijing 100193, China

noise ratio due to self-quenching and photobleaching [14]. To eliminate the loss of fluorescence, sensitizers have now been introduced into the fluorescence system [11, 15]. However, this method has increased the complexity of detection. Moreover, it is hard to improve the sensitivity if several fluorophores are loaded onto proteins within a confined space.

To overcome these limitations, a 'turn-on' approach using self-assembled aptamers was preferred for biosensing trace contaminates [16, 17]. This method is heavily relied on the special structures of pesticides, which were valid on ligand-replacement [18, 19]. This method is hard to be expanded to a wide application field, and it is seldom employed in immunoassays. Generally, nanogold-based platforms, [20, 21] which are triggered with a switch to turn on the fluorescent signal, would significantly enhance the signal-to-noise ratio.

Nanogold has advantages such as perfect fluorescence quenching [22, 23], large specific surface area, strong absorption and compatibility with biomolecules. Nanogold release from functionalized fluorophore complexes was employed to yield a sensitive cyanide assay with a limit of detection (LOD) below 1.0 μM [24]. Alternatively, Liu et al. [25] designed a recyclable Hg^{2+} probe below a LOD of 3.0 nM, principally attributed to the sensitive displacement of Rhodamine B isothiocyanate (RBITC) from nanogold. The turn-on pattern-based immunoprobes possess attractive potential for contaminant detection. However, it is not employed and fully developed to now.

In this study, a labeled probe was fabricated through binding both RBITC and IgG on nanogold, leading to fluorescence quenching effect. Based on a turn-on scheme, an ingenious monitoring platform was designed by competitive readouts using the nanoprobe. This readout was due to RBITC release from the nanogold's surface via ligand replacement by a stronger ligand—cysteamine. Due to effective quenching and abundant loads of dyes onto the nanogold, the signal-to-noise ratio was expected to be effectively improved by employing this technique. Using chlorpyrifos as a model, the turn-on scheme was implemented on a microplate, and the detection performance was further validated by conventional LC-MS/MS measurements.

Experimental section

Materials and instruments

Trisodium citrate dehydrate and chloroauric acid tetrahydrate ($HAuCl_4 \cdot 4H_2O$, 99%) were obtained from Sinopharm Chemical Reagent Co., Ltd. (Shanghai, China). Bovine serum albumin (BSA) and chicken ovalbumin (OVA) were purchased from Shi Huier Biological Technology Co., Ltd. (Yangzhou, China). Goat serum (GS) was from Beijing Hapten and Protein Biomedical Institute. Nonfat dry milk (NDM) was purchased from Inner Mongolia Yili Industrial Group Co., Ltd. Goat Anti-Mouse Ig (IgG) and fluorescein isothiocyanate labeled IgG (FITC-IgG) were from Nanning blue light biotechnology Inc. Chlorpyrifos (CP), alachlor, propamocarb, acetochlor, atrazine, benomyl, bromacil, 3, 5, 6-Trichloro-2-pyridinol and metolachlor standards were purchased from Agriculture Environment Quality Supervision, Inspection, and Testing Center (Tianjin, China). Chlorpyrifos-BSA (CP-BSA) and anti-CP monoclonal antibody were provided by Wanhua Bioresearch & Technology Co., Ltd. (Beijing, China). Cysteamine was from Adamas Reagent Co., Ltd. Rhodamine B Isothiocyanate (RBI) was from Shanghai Aladdin Bio-chem Technology. All the reagents were of analytical grade. Deionized water used throughout the experiments was purified by a Milli-Q system (Millipore, CA).

The gold nanoparticles were characterized by JEM-1200EX Transmission electron microscopy (TEM, JEOL, Japan). UV-vis spectrum was measured for gold nanoparticles by using an Agilent Cary 100 UV-Vis spectrophotometer (Agilent, USA). Fluorescence data were recorded by a microplate reader (Infinite® M1000 pro, Switerland, Tecan Company). Sonication was conducted with a KQ-500 ultrasonicer (Kunshan, China). The hydrodynamic radius was analyzed by Dynamic Light Scattering (DLS) and the surface charge was through Zeta Potential on Zetasizer Nano ZS equipped with Zetasizer Software (Malvern, UK). Liquid chromatography coupled with tandem mass spectrometer (LC-MS/MS, AB SCIEX, QTRAP® 5500, USA) analysis was performed on an AQUITY UPLC BEH Shield RP18 column (100 × 2.1 mm, 1.7 μm). The ion transitions of 350.1 → 197.9 and 350.1 → 96.9 were used to identify and quantify chlorpyrifos, respectively.

Surface-assembly of the gold-RBITC-IgG probe

Prior to assembly, the nanogold (see supporting information) was concentrated twenty times using ultracentrifugation. The resulting precipitate was then redispersed in deionized water. To facilitate immobilization, the mixture was adjusted to pH 9.0 using 100 mM K_2CO_3. Afterwards, 4 μL of 10 mM RBITC was added under gentle agitation for 1 h in the dark. Any excess reagents were removed using two cycles of ultracentrifugation and the conjugate was then redissolved in 2 mM K_2CO_3. After dissolving, an aliquot was taken to characterize its structural properties with UV-Vis, ZP and DLS measurements. Further IgG immobilization was performed with the addition of 10 $mg \cdot mL^{-1}$ IgG (20 μL), which was then gently agitated for 2 h in the dark. After the reaction, the remaining active sites on the probe were blocked with 1% BSA for 30 min. The final probe was purified by washing twice with phosphate-buffered saline containing 0.05%Tween-20 (PBST). The probe was redissolved in 1 mL PBST at 4 °C and stored in the dark for later use.

Sample preparation

In the assay, dried tangerine peel powder (1.0 g) was weighed and immersed in 5 mL of a mixed solvent of methanol and water (with a volume ratio of 4:1). The solution was vigorously shaken for 1 min and ultrasonicated for 5 min. The mixture was then centrifuged for 5 min at 4000 rpm. An aliquot of extract (2 mL) was concentrated to 0.5 mL under nitrogen flow and then resuspended in PBS containing 10% methanol. After subsequent centrifugation, the precipitate was discarded and the supernatant was diluted five times with 10% methanol-PBS and adjusted to pH 7.0–7.5 using 1 M NaOH.

Labeled monitoring platform

Black 96-well polystyrene microplates were modified by coating with 200 μL of CP-BSA (625 ng·mL^{-1}) in carbonate buffer (pH 9.6) at 4 °C overnight. After washing three times with phosphate-buffered saline (PBS) containing 0.05% Tween-20 (PBST), plates were blocked with 2% BSA in PBS at 37 °C for 2 h. Plates were then washed twice with PBST, after which 50 μL of sample solution and anti-CP antibody in PBS solution (1: 8000) were separately added in sequence, and incubated at 37 °C for 1 h. Afterwards, the remaining analyte-antibody complex solution was discarded and the plates were washed three times with PBST. Au-RBITC-IgG probe in PBS (1:50) was then added to the reacted wells followed by incubation at 37 °C for 30 min. After washing with PBST and water, 50 mM cysteamine (100 μL) was then added to the plates and they were subjected to shaking for 1 min. Fluorescence measurements were performed using a microplate reader with excitation (λ_{ex}) at 556 nm and emission (λ_{em}) at 575 nm. Comparative experiments were conducted using LC-MS/MS according to our previously published methods [26] (Sample preparation was referred to Supplementary Information) and traditional fluorescent immunoassay (FIA). Instead of Au-RBITC-IgG probe in this dual-labeled immunoassay, FIA applied 1: 2000 of FITC-IgG to recognize and marker the antibody remained in plates. After washing by PBST, the fluorescence was recorded at 495 nm of λ_{ex} and 520 nm of λ_{em} with addition of 100 μL of PBS.

Results and discussion

Principle of the labeled monitoring platform

RBITC was intensively used as a protein fluorophore tag [27, 28]. As shown in Fig. 1a, the dye contains both unique isothiocyano (ITS, −N = C = S) and quaternary ammonium $[CH_2CH_3]_2N^+$ groups, which was the foundation for a labeled conjugate. After two synthetic steps diagrammed in Fig. 1a, the Au-RBITC-IgG conjugate was accomplished. Due to the π-conjugated form on the surface of gold (the rich π-electrons provided by the anchoring group of ITS), the poor adsorption of citrate ($C_5H_7O_5COO^-$) was first displaced from the nanogold surface by RBITC and it enabled strong electronic coupling between the adsorbed dye-RBITC and nanogold [29, 30]. The IgG protein was then readily assembled to RBITC-Au via an electrostatic attachment domain between $[CH_2CH_3]_2N^+$ and IgG [31]. Using the Au-RBITC-IgG conjugate as a tracer, a schematic representation of the labeled monitoring platform is outlined in Fig. 1b. The platform is based on an indirect competitive fluorescent immunoassay, followed by competitive readouts using the nanoprobe. The detail workflow was as follows: (1) The 96-plate wells were immobilized with antigen, then sample solution and primary antibody were added in turn. (2) Competitive reaction between immobilized antigen and target in sample led to limited primary antibodies remaining on the well. (3) The nanoprobe labeled the remaining primary antibodies through recognition of IgG to primary antibodies. (4) After addition of cysteamine, RBITC dyes were released from the nanoprobe and boosted a fluorescence signal due to the stronger binding of cysteamine with nanogold than RBITC dyes. Prior to the addition of cysteamine, the absolute fluorescence quenching of RBITC was attributed to its binding with the nanogold [32]. It resulted from fluorescence resonance energy transfer, because it satisfied the necessity for an approximate distance, a broad absorption spectrum and strong extinction coefficient [33]. The presence of a small molecule like cysteamine allowed for easy exchange of the IgG-RBITC capping on the nanogold. This was due to the high binding ability of Au-S. The release of RBITC in solution led to a significant enhancement of fluorescence intensity. Based on the competitive assay used with the method, the amounts of included tracer remaining in the well can indicate the recognition activities of IgG bound to primary antibody. Chlorpyrifos levels were inversely proportional with the amounts of the tracer. In comparison with either the HRP-IgG or dye-IgG, Au-RBITC-IgG was employed as a promising alternative for use as an indirect reaction tracer.

Characterization of the gold-RBITC-IgG probe

The desired nanogold had both excellent stability and morphology and laid the foundation for the final probe construction. As shown in Fig. S1, the synthetic gold nanoparticles show a typical absorption band at 518 nm and are approximately 20 nm in diameter. They also had robust monodisperse properties. To confirm the conjugation process of the Au-RBITC-IgG probe, dynamic light scattering (DLS) measurements were conducted. The hydrodynamic radius of Au-RBITC increases from 24 ± 0.27 nm to 40.9 ± 1.13 nm (n = 3) due to RBITC immobilization on the nanogold surface (Fig. 2a). The large molecular radius of IgG meant that the overall radius is enlarged to 115.5 ± 1.41 nm (n = 3).

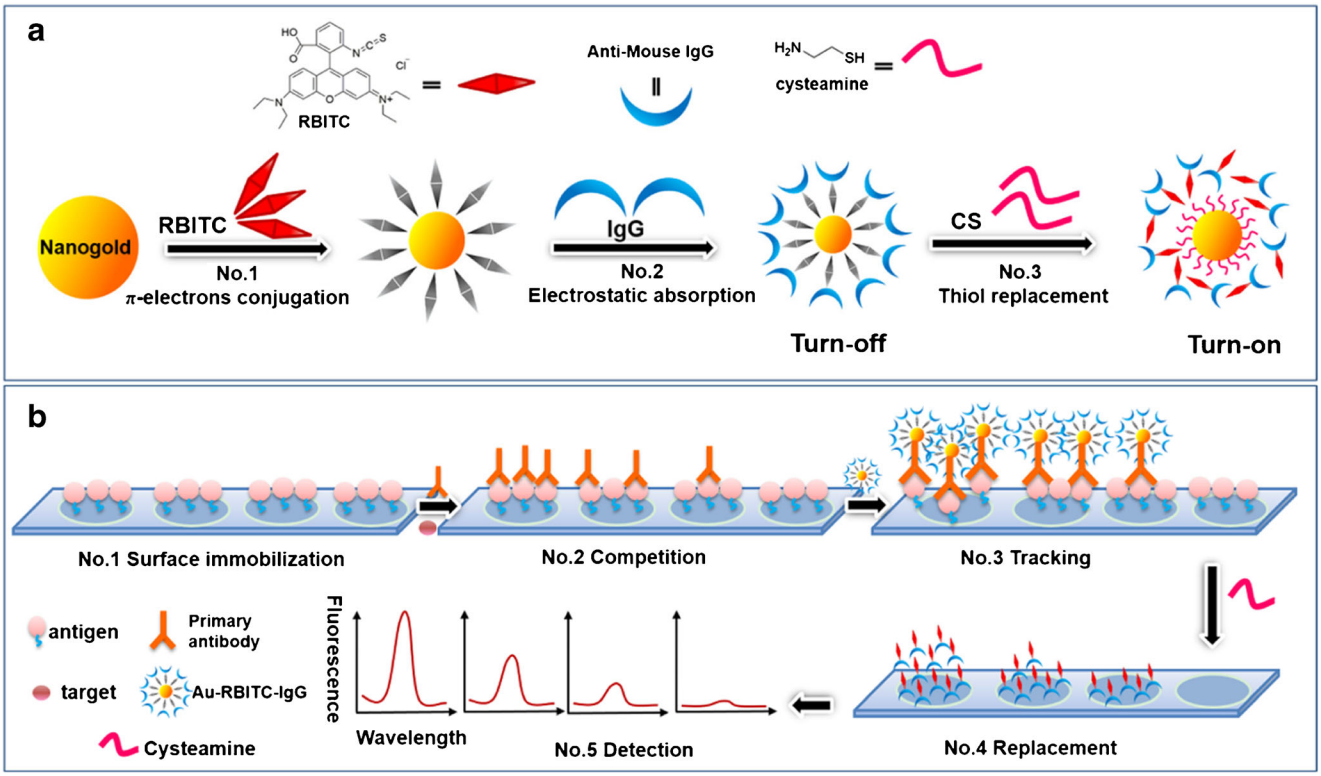

Fig. 1 Fabrication of the labeled nanoprobe **a** and schematic illustration of labeled monitoring platform **b**

Interestingly, the probe tagged with IgG possesses a narrow dispersion scope of 0.14 ± 0.01 ($n = 3$), which would facilitate good reproducibility in assay. The completed probe is further supported by zeta potential (ZP) data ((Fig. 2b), which reveals a markedly decreased value when compared with either pure nanogold or the Au-RBITC conjugate. These results indicate that RBITC and IgG were conjugated in a layer-by-layer fashion to the nanogold.

Feasibility of the assay

Visible absorption scanning spectra for pure nanogold, RBITC, Au-RBITC conjugate serials are presented in Fig. 3a. The probe presents characteristic peak at 518 nm from nanogold and peak at 558 nm from RBITC, respectively. In the presence of cysteamine, the absorption of Au-RBITC-IgG revealed a comparable spectrum to that of free RBITC due to the released fluorophore. The nanogold surrounded with new ligand appeared to aggregate, resulting in a redshifted peak at 650 nm. In addition, the 'turn-on' strategy was validated by sunlight and UV lamp exposure to investigate the color change. As shown in Fig. 3b, the color of the conjugate and free nanogold under sunlight present purplish red and bright red, respectively. When cysteamine is included in the solution, it immediately turns to clear pink. The recovery of orange fluorescence and a dark tonality were easily distinguished both before and after being 'turned-on' by cysteamine. It is possible that quenching is due to unbound RBITC and nanogold. However,

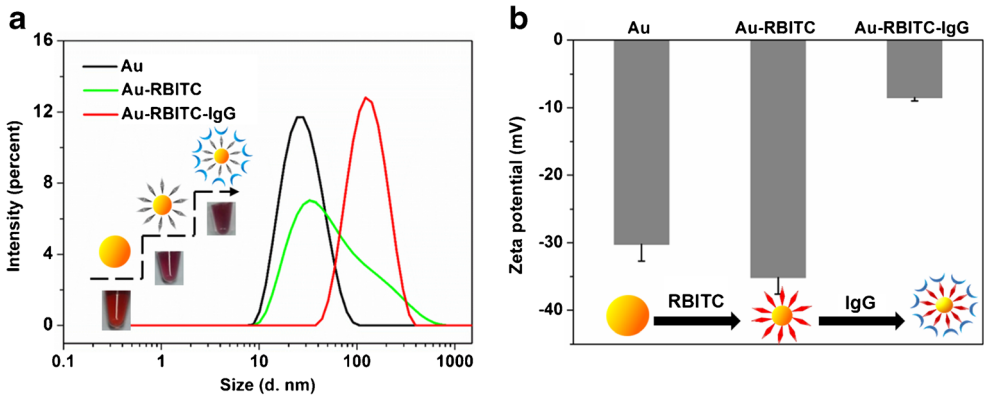

Fig. 2 Hydrodynamic size distribution **a** and the surface charge **b** of nanogold, Au-RBITC conjugate, and the labeled probe measured by dynamic light scattering and zeta potential

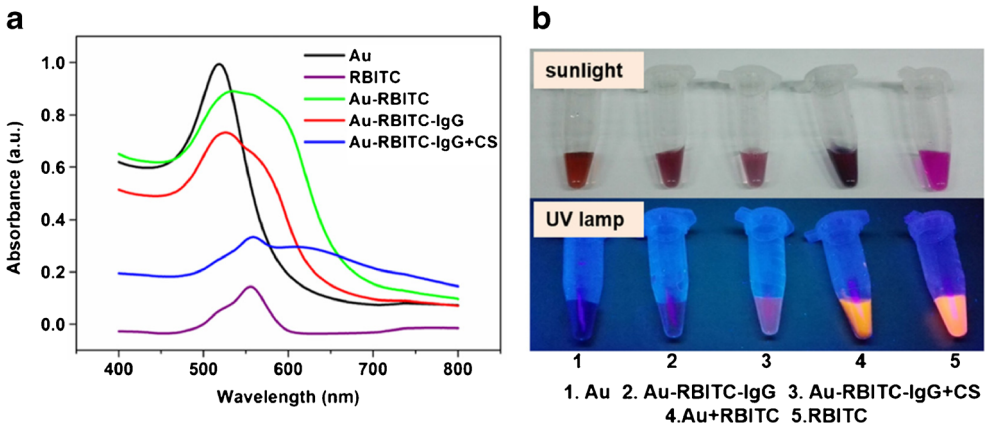

Fig. 3 Visible absorbance spectrum **a** and images taken under sunlight and UV lamp **b** for pure nanogold and RBITC, Au-RBITC conjugate, completed probe, and probe mixed with cysteamine

the fluorescence of the Au + RBITC group was like the RBITC solution, while the probe was much different from the mixture. Therefore, these results indicate that fluorescence quenching was derived from the combined Au-RBITC-IgG.

Interference study with the fluorescence platform

To implement labeled immunoprobe in routine analysis after critical parameters optimization (Fig. S2-S5), it is essential to study interference effect of the possible contaminants and interference found in real samples on the fluorescence platform. To investigate the anti-interference ability, the method was applied for the detection of chlorpyrifos in dried tangerine peels. Dried tangerine peel is a popular is a popular ingredient in spices, condiments, snack food, and tea that is used in great quantities. Previous reports have indicated chlorpyrifos is among the most frequent and hazardous contaminant found in tangerines, including in their peels [26, 34, 35].

In our first experiment, we used direct extract without further dilution or pH adjustment. Results show an apparent matrix suppression effect when compared with analyte prepared using pure solvent (Fig. 4a, see red line). The possible reason mainly is that the matrix (including pH below 3.5 and interference with concentrated co-extract) affects the reaction between antibody and antigen. Given these, the hypothesis is validated and the previously seen matrix suppression is greatly improved (Fig. 4a, see blue line). After pretreatment with dilution and pH adjustment, the extracted matrix has a negligible effect on detection, leading to reliable and quantitative results. Furthermore, this result also suggested that the method has promise for the quantification of a small target in a complex mixture.

Analytical performance including dynamic range, sensitivity, accuracy and specificity

Using these optimal conditions, a dilution series of a known standard was performed to determine the dynamic range for the labeled monitoring platform and traditional FIA. A blank, analyte-free diluent was used as the control group. An inhibition curve for the analyte was constructed by plotting fluorescence inhibition against the target concentration. Fluorescence inhibition was calculated. The dose-dependent inhibition curve is shown in Fig. 4a (see black line). We defined 10% fluorescence inhibition as the lowest detected concentration, thus allowing the assay an allows a limit of detection (LOD) of 4.88 ng·mL^{-1} (coefficient of variation, CV < 2%). This corresponds to a concentration of 0.061 mg·kg^{-1} in dried tangerine peel, which satisfies the required maximum standard of 0.2–2 mg·kg^{-1} of chlorpyrifos in the related food regulations. The IC_{50} was defined as 50% fluorescence inhibition and is found to be 87.8 ng·mL^{-1}. The dynamic range was determined as the analyte concentration generating between 20% and 80% of maximal inhibition. As shown in Fig. 4b, the labeled system exhibits excellent linearity (a correlation coefficient of 0.9953) within the range of 1250–9.77 ng·mL^{-1} with a calibration curve of $Y = 27.78\text{LogC}-3.997$. It is observed that the high values obtained for the standard deviation in the upper zone of the calibration graph. The deviation might result from the unevenly bound dye, RBITC. It cannot be evenly dispersed and bound on the surface of nanogold. The compared FIA shown in Fig. S6 indicates the reliable IC_{50} for chloropyrifos residue is 63.1 ng·mL^{-1}, whereas the dynamic curve is $Y = 32.71\text{LogC}-8.884$ (a correlation coefficient of 0.9892) in the concentration range of 625–9.77 ng·mL^{-1}. Above results suggested although both of them displayed a similar IC_{50} and limit detection, the turn-on strategy had superior dynamic range and correlation coefficient for the relationship between concentration and response.

Critically, the broad dynamic range and perfect linearity seen in these data are solely attributable to the labeled scheme. To this end, the turn-on strategy allowed for the fluorophore to be released in the final step. This allowed for the avoidance of photobleaching and subsequent signal enhancement. In addition, each labeled nanogold loaded many reporters, thus leading to the fluorescence amplification over multiple orders of magnitude. This also facilitated the improved signal-to-noise ratio. This finding also indicates that the labeled probe using cysteamine provides amplification approach to the conventional biotin-streptavidin system.

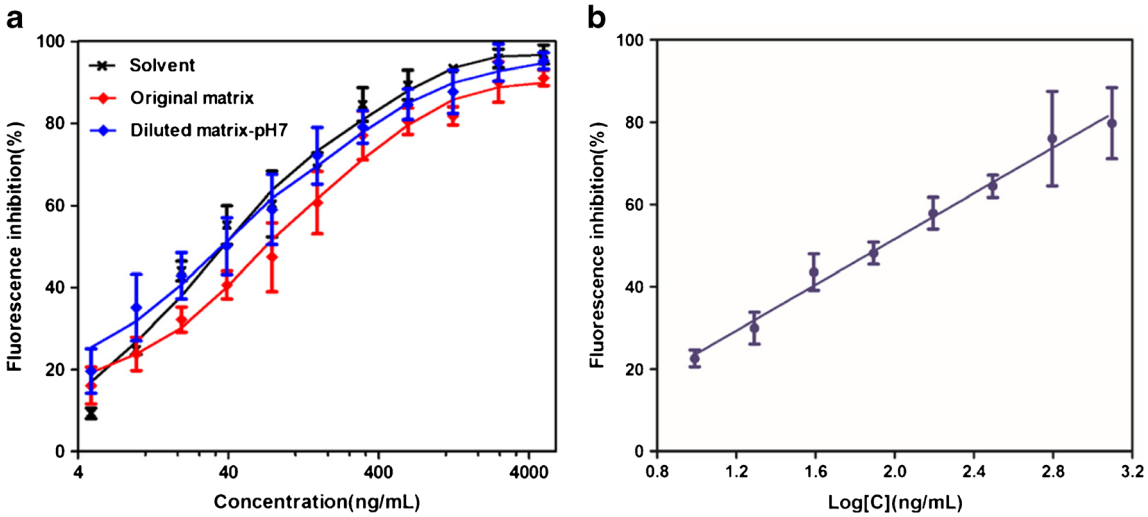

Fig. 4 Fluorescence inhibition curves **a** of chloropyrifos prepared in pure solvent (black line), matrix with no dilution (red line), and matrix with dilution (blue line) and corresponding calibration curve **b** for immunoassay based on labeled probe. The fluorescence was recorded with a wavelength of excitation at 556 nm and emission at 575 nm. Error bars are standard deviation for three parallel tests

Accuracy was next examined using the recovery of spiked tangerine peel at 1 $\mu g \cdot g^{-1}$, approximating the previously determined IC_{50}. Six parallel samples were prepared and determined by the method. Resulting levels in the spiked samples were then quantified using the calibration curve. The calculated recovery value and CV are 83.7 ± 5.4% and 6.2%, respectively. The spiked sample test was repeated six times per day and on three consecutive days to evaluate both the inter-day and intra-day variability. The inter- and intra-assay CVs evaluated are 3.6% and 4.7%, respectively. These results were within specified ranges, thus indicating that our novel method had both high loading efficiency of the fluorophore as well as an excellent ability to turn-on fluorescence. This makes it a more efficient and simpler operation that still has good performance. Specificity were investigated with similar chemicals including chlorfenvinphos, bromophos-ethyl, dichlofenthion, chlorpyrifos-methyl and 3, 5, 6-Trichloro-2-pyridinol with each concentration level at 100 $ng \cdot mL^{-1}$. The fluorescence inhibition was calculated and all of those displayed fluorescence inhibition is within 7.2 ± 0.3% ($n = 3$). Thus, those analogues had an ignored interference on the targets detection. The result indicates that the method possesses an excellent selective for chlorpyrifos over other pesticides. After a stability test, the probe can keep effective for a half month during storage in black at 4 °C. When it was prepared to use in the labelled monitoring platform, the solution just required to return to room temperature and a gentle shake to make sure it disperse homogeneously.

Real sample analysis using the fluorescent immunoassay

To better understand the efficiency of our labeled approach versus conventional methods, fifteen incurred and two negative dried tangerine peels were analyzed using both the monitoring platform and LC-MS/MS method. Each sample was analyzed in triplicate and levels were determined using the calibration curve. Among them, twelve identified by the method exceeds the limit standard of 0.2 $mg \cdot kg^{-1}$, two and one samples are below LOD and LOQ, respectively. According to our previous study, the complicated extract required a clean-up process prior to LC-MS/MS analysis. The

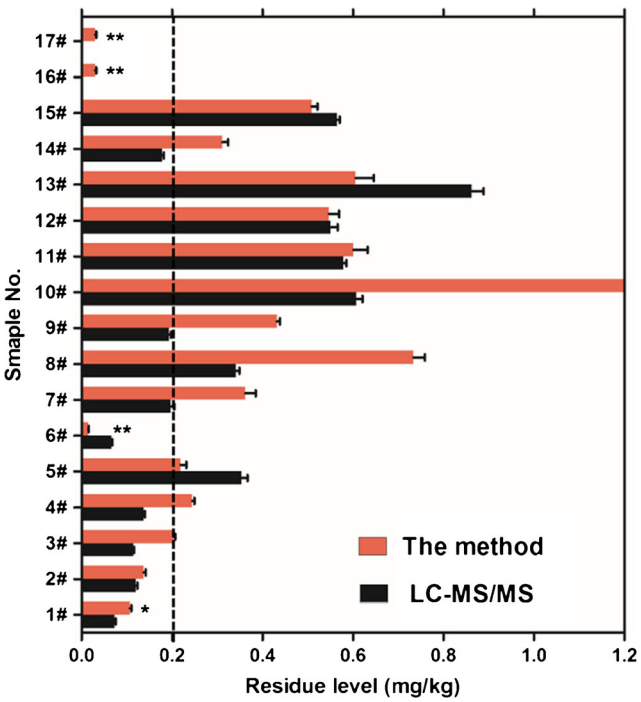

Fig. 5 Comparison of chlorpyrifos residue levels in seventeen dried tangerine peels using the dual-labeled method and conventional LC-MS/MS method. (** represents not detected, while * represents the level above the limit detection but below the quantification limit)

fourteen positive samples identified by the labeled assay were confirmed with two different ion channels using LC-MS/MS. Moreover, results indicate that the residue levels from the novel method presented here compared favorably with those from the conventional, LC-MS/MS approach (Fig. 5). Although the LC-MS/MS method has high sensitivity and accuracy, the labeled method, as an explorative method, can be applied for pesticide determination in real samples with uncomplicated pretreatment procedures and enough selectivity. Nevertheless, when dealing with samples rich in pigment, acid or alkaline matrices, these substances may interfere the sensitivity and effectiveness of this method by using the labeled assay. Further sample preparation probably was required to avoid generating positive results.

Conclusion

In summary, a labeled probe employing a fluorescence turn-on scheme was designed to indirectly mark analyte residue in our monitoring platform. The labelled antibody was synthesized by modifying gold nanoparticles with the fluorophore rhodamine B isothiocyanate and a secondary antibody. The conjugate was used to detect the organophosphorus pesticide chlorpyrifos. This approach can decrease fluorescence losses and improve the linearity range of the ordinary fluorescence immunoassay through nanogold-driven signal amplification. The labelled antibody was effective and sensitive in detecting chlorpyrifos in tangerine peels with a satisfying detection limit far below the maximum residual level. In addition, the results were also validated by the LC-MS/MS measurements. In our perception, this approach has a wide potential to be applied in the determination of numerous analytes for which antibodies are available. Nevertheless, when dealing with samples rich in pigment, acid or alkaline matrices, these substances may interfere the sensitivity and effectiveness of this method by using the labeled assay. More work need to be carried out to improve this method in future.

Acknowledgements The work was supported by National Natural Science Foundation of China (81573595, 81703699), National Project for Standardization of Chinese Materia Medica (ZYBZH-Y-JIN-34), CAMS Innovation Fund for Medical Sciences (2016-I2M-1-012, 2016-I2M-3-010, 2017-I2M-1-013).

Compliance with ethical standards The author(s) declare that they have no competing interests.

References

1. Nakano VE, Kussumi TA, Lemes VRR, Kimura IA, Rocha SB, Alaburda J, Oliveira MCC, Ribeiro RA, Faria ALR, Waldhelm KC (2016) Evaluation of pesticide residues in oranges from São Paulo. Brazil Food Sci Technol (Campinas) 36:40–48
2. Liu Y, Li S, Ni Z, Qu M, Zhong D, Ye C, Tang F (2016) Pesticides in persimmons, jujubes and soil from China: residue levels, risk assessment and relationship between fruits and soils. Sci Total Environ 542:620–628
3. Sadowska-Rociek A, Surma M, Cieślik E (2013) Application of QuEChERS method for simultaneous determination of pesticide residues and PAHs in fresh herbs. Bull Environ Contam Toxicol 90(4):508–513
4. Aragay G, Pino F, Merkoçi A (2012) Nanomaterials for sensing and destroying pesticides. Chem Rev 112(10):5317–5338
5. Arduini F, Cinti S, Scognamiglio V, Moscone D (2016) Nanomaterials in electrochemical biosensors for pesticide detection: advances and challenges in food analysis. Microchim Acta 183(7):2063–2083
6. Wang X, Cao Y, Chen D, Zhao G, Sun X (2014) An amperometric immunosensor based on graphene composite film and protein a for chlorpyrifos detection. Sensors Trans 178(9):47–55
7. Sun, Z, Wang, W, Wen, H, Gan, C, Lei, H and Liu, Y (2015) Sensitive electrochemical immunoassay for chlorpyrifos by using flake-like Fe3O4 modified carbon nanotubes as the enhanced multienzyme label. Anal Chim Acta 899 (Supplement C): 91–99
8. Xu ZL, Wang Q, Lei HT, Eremin SA, Shen YD, Wang H, Beier RC, Yang JY, Maksimova KA, Sun YM (2011) A simple, rapid and high-throughput fluorescence polarization immunoassay for simultaneous detection of organophosphorus pesticides in vegetable and environmental water samples. Anal Chim Acta 708(1–2):123–129
9. Beloglazova NV, Speranskaya ES, Wu A, Wang Z, Sanders M, Goftman VV, Zhang D, Goryacheva IY, De Saeger S (2014) Novel multiplex fluorescent immunoassays based on quantum dot nanolabels for mycotoxins determination. Biosens Bioelectron 62: 59–65
10. Goldman, ER, Anderson, GP, Lebedev, N, Lingerfelt, BM, Winter, PT, Patterson, CH, Jr. and Mauro, JM (2003) Analysis of aqueous 2, 4,6-trinitrotoluene (TNT) using a fluorescent displacement immunoassay. Anal Bioanal Chem 375(4): 471–475
11. Petrou PS, Mastichiadis C, Christofidis I, Kakabakos SE (2007) Glycerin suppression of fluorescence self-quenching and improvement of heterogeneous Fluoroimmunoassay sensitivity. Anal Chem 79(2):647–653
12. Tang D, Yu Y, Niessner R, Miro M, Knopp D (2010) Magnetic bead-based fluorescence immunoassay for aflatoxin B1 in food using biofunctionalized rhodamine B-doped silica nanoparticles. Analyst 135(10):2661–2667
13. Feng J, Shan G, Maquieira A, Koivunen ME, Guo B, Hammock BD, Kennedy IM (2003) Functionalized europium oxide nanoparticles used as a fluorescent label in an immunoassay for atrazine. Anal Chem 75(19):5282–5286
14. Viger ML, Live LS, Therrien OD, Boudreau D (2008) Reduction of self-quenching in fluorescent silica-coated silver nanoparticles. Plasmonics 3(1):33–40
15. Sharma P, Gandhi S, Chopra A, Sekar N, Raman Suri C (2010) Fluoroimmunoassay based on suppression of fluorescence self-quenching for ultra-sensitive detection of herbicide diuron. Anal Chim Acta 676(1–2):87–92
16. Wang Z, Heon Lee J, Lu Y (2008) Highly sensitive "turn-on" fluorescent sensor for Hg2+ in aqueous solution based on structure-switching DNA. Chem Commun (Camb) 45:6005–6007
17. Lin B, Yu Y, Li R, Cao Y, Guo M (2016) Turn-on sensor for quantification and imaging of acetamiprid residues based on quantum dots functionalized with aptamer. Sensors Actuators B Chem 229: 100–109
18. Zhang J, Wang J, Yang L, Liu B, Guan G, Jiang C, Zhang Z (2014) Ligand replacement induced chemiluminescence for selective detection of an organophosphorus pesticide using bifunctional au-

Fe3O4 dumbbell-like nanoparticles. Chem Commun 50(100): 15870–15873
19. Zhang K, Mei Q, Guan G, Liu B, Wang S, Zhang Z (2010) Ligand replacement-induced fluorescence switch of quantum dots for ultrasensitive detection of Organophosphorothioate pesticides. Anal Chem 82(22):9579–9586
20. Wang Q, Jin Y, Fu X, Ma M, Cai Z (2016) A "turn-on-off-on" fluorescence switch based on quantum dots and gold nanoparticles for discriminative detection of ovotransferrin. Talanta 150:407–414
21. Zhu J, Chang H, Li JJ, Li X, Zhao JW (2017) Dual-mode melamine detection based on gold nanoparticles aggregation-induced fluorescence "turn-on" and "turn-off" of CdTe quantum dots. Sensors Actuators B Chem 239:906–915
22. Maxwell DJ, Taylor JR, Nie S (2002) Self-assembled nanoparticle probes for recognition and detection of biomolecules. J Am Chem Soc 124(32):9606–9612
23. Dubertret B, Calame M, Libchaber AJ (2001) Single-mismatch detection using gold-quenched fluorescent oligonucleotides. Nat Biotechnol 19(4):365–370
24. Shang L, Jin L, Dong S (2009) Sensitive turn-on fluorescent detection of cyanide based on the dissolution of fluorophore functionalized gold nanoparticles. Chem Commun (Camb) 21:3077–3079
25. Liu D, Wang S, Swierczewska M, Huang X, Bhirde AA, Sun J, Wang Z, Yang M, Jiang X, Chen X (2012) Highly robust, recyclable displacement assay for mercuric ions in aqueous solutions and living cells. ACS Nano 6(12):10999–11008
26. Dou X, Chu X, Kong W, Yang Y, Yang M (2015) Carbon nanotube-based QuEChERS extraction and enhanced product ion scan-assisted confirmation of multi-pesticide residue in dried tangerine peel. RSC Adv 5(105):86163–86171
27. Wang, J, Li, H, Zou, H, Wang, C, Zhang, H, Mano, JF and Song, W (2017) Flexible method for fabricating protein patterns on superhydrophobic platforms controlled by magnetic field. Biomater Sci 5(3):408–411
28. Shahabi S, Treccani L, Dringen R, Rezwan K (2015) Dual fluorophore doped silica nanoparticles for cellular localization studies in multiple stained cells. Acta Biomater 14:208–216
29. Qian X, Emory SR, Nie S (2012) Anchoring molecular Chromophores to colloidal gold Nanocrystals: surface-enhanced Raman evidence for strong electronic coupling and irreversible structural locking. J Am Chem Soc 134(4):2000–2003
30. Qian X, Peng X-H, Ansari DO, Yin-Goen Q, Chen GZ, Shin DM, Yang L, Young AN, Wang MD, Nie S (2008) In vivo tumor targeting and spectroscopic detection with surface-enhanced Raman nanoparticle tags. Nat Biotechnol 26(1):83–90
31. Liu D, Huang X, Wang Z, Jin A, Sun X, Zhu L, Wang F, Ma Y, Niu G, Hight Walker AR, Chen X (2013) Gold nanoparticle-based Activatable probe for sensing ultralow levels of prostate-specific antigen. ACS Nano 7(6):5568–5576
32. Manju S, Sreenivasan K (2011) Detection of glucose in synthetic tear fluid using dually functionalized gold nanoparticles. Talanta 85(5):2643–2649
33. Ray PC, Darbha GK, Ray A, Walker J, Hardy W (2007) Gold nanoparticle based FRET for DNA detection. Plasmonics 2(4): 173–183
34. Angioni A, Dedola F, Garau A, Sarais G, Cabras P, Caboni P (2011) Chlorpyrifos residues levels in fruits and vegetables after field treatment. J Environ Sci Health B 46(6):544–549
35. Golge O, Kabak B (2015) Determination of 115 pesticide residues in oranges by high-performance liquid chromatography–triple-quadrupole mass spectrometry in combination with QuEChERS method. J Food Compos Anal 41:86–97